

Chapter 3

INFLUENCE OF CONFIGURATIONAL DISORDER ON THE INTRINSIC FRACTURE TOUGHNESS OF METALLIC GLASSES

ABSTRACT

The effect of the configurational disorder of the glass structure on the intrinsic fracture toughness of metallic glasses is explored. The fracture toughness measured in as-quenched and well-defined relaxed configurations is correlated with measured elastic constants and recovered enthalpy in an effort to quantify the influence of configurational disorder on toughness. The as-quenched glass is found to exhibit a broadly varying toughness that cannot be correlated to the average configurational properties, and is thought to arise from a large configurational disorder captured in the as-quenched state. In contrast, the glass equilibrated at well-defined configurations demonstrates a consistent toughness that is systematic and correlatable to the average configurational properties. The large configurational disorder in the as-quenched state responsible for the wide toughness variance is attributed to a dynamic vitrification process capturing a broad spectrum of unrelaxed modes; the spectrum narrows significantly following relaxation of the glass, promoting more consistent toughness.

INTRODUCTION

Toughness in metallic glasses is accommodated by a mechanism of highly localized plastic flow, known as shear banding, originating at the crack tip. Shear bands blunt the crack tip and shield it from the applied opening stress, and in instances when extensive shear banding is enabled, crack growth may be entirely arrested [1]. Shear banding is an intrinsic toughening mechanism taking place solely in the material ahead of the crack tip [2]. Specifically, energy is dissipated when the local elastic stress in front of the crack tip is large enough to overcome the activation barrier for shear flow (i.e., the stress reaches the plastic yield strength) such that shear bands are nucleated inside the region called the “plastic zone.” The larger the density of shear bands and the longer those shear bands slide within the plastic zone before cavitation intervenes to facilitate crack extension, the larger the plastic zone and the greater the toughness of the material. The extent to which the glass can undergo shear banding in the absence of cavitation ahead of the crack tip is intimately related to the local configurational properties of the glass in the immediate vicinity of the crack tip.

The toughness of metallic glasses is known to vary greatly between the different compositional families, ranging from very high for noble-metal glasses (up to $200 \text{ MPa}\cdot\text{m}^{1/2}$) [1], to moderately high for early-transition metal glasses ($\sim 100 \text{ MPa}\cdot\text{m}^{1/2}$) [3], to very low for ferrous metal glasses (under $10 \text{ MPa}\cdot\text{m}^{1/2}$) [4]. But considerable variability in toughness is often reported for the same metallic glass composition. For example, a thorough investigation by Kawashima et al. [5] using 35 specimens revealed a significant variation in the fracture toughness of $\text{Zr}_{55}\text{Ni}_5\text{Cu}_{30}\text{Al}_{10}$ ranging from 36 to

76 MPa·m^{1/2}. A comparable scatter was also reported for Zr_{52.5}Ti₅Ni_{14.6}Cu_{17.9}Al₁₀ [6]. In both of these studies, the scatter was attributed to extrinsic factors such as partial crystallinity or inclusions. These inhomogeneities tend to precipitously drop toughness when intersected by a propagating crack, thus widening the scatter in the measured toughness. Their intersection with a crack is typically associated with a change in fracture mode, displaying a cleavage fracture region in the crack wake. In brittle metallic glasses the effect of oxide inclusions is much more profound, as it essentially dominates the fracture resistance of those glasses [7,8]. Yet a large variability in toughness is often reported for glasses that are relatively tough and expected to be generally insensitive to inclusions. Even when processed under near-ideal conditions (high-purity and low-oxygen content elements, highly-inert atmosphere) that restrict the formation of oxide inclusions, and are fully amorphous as verified by careful X-ray diffractometry, such tougher glasses still often display a large variation in toughness. For example, the fracture toughness of pristine Zr_{41.2}Ti_{13.8}Ni₁₀Cu_{12.5}Be_{22.5} samples processed under essentially identical conditions was found to vary from a low value of 25 MPa·m^{1/2} to a high value of 75 MPa·m^{1/2}, while no visible inhomogeneities could be detected in the fracture morphology to suggest influence by extrinsic factors [9]. This suggests that significant variability in toughness may also be caused by intrinsic factors at much shorter length scales associated with local inhomogeneities in the glassy structure.

Structural relaxation is known to profoundly affect the toughness of metallic glass. Gradually relaxing the glass from the highly-disordered as-quenched state to a well-defined equilibrium state at a temperature lower than the fictive temperature associated with the as-

quenched state is found to severely compromise toughness [10,11]. This is understood to be a consequence of relaxing at a lower level in the potential energy landscape, associated with a higher barrier for shear flow as compared to the as-quenched state [12]. As those previous investigations always involve a change in the fictive temperature, any effects of the decrease in the degree of disorder on going from the highly disordered as-quenched state to a less disordered equilibrium state are not addressed. A recent computational work suggests that the degree of disorder can have quite a significant effect on toughness, perhaps as significant as the effect of varying the fictive temperature [13]. In the present study, we experimentally isolate the effect of varying glass disorder from the effect of changing the fictive temperature and attempt to independently examine their respective effects on toughness.

The average configurational properties and fracture toughness are measured for several specimens in the as-quenched state as well as in states relaxed at various temperatures around the glass transition. A relaxation temperature that closely approximates the fictive temperature of the as-quenched state is determined by correlating the respective configurational properties. Comparing the toughness for relaxed and as-quenched states at approximately the same fictive temperature enables, for the first time, assessment of the effects of glass disorder on fracture toughness. In order to obtain an accurate representation of the average configurational properties ahead of the crack tip plane such that valid correlations with fracture toughness are enabled, ultrasound measurements were taken just ahead of the crack tip through the thickness of each sample. In order to circumvent the unpredictable adverse effects on toughness of either crystallinity

or inclusions, each tested sample was prepared with diligent care and was thoroughly inspected. The fully amorphous nature of the tested samples was carefully inspected by X-ray diffraction and differential scanning calorimetry. The alloy ingots were prepared using high-purity elements with low oxygen content, alloyed under ultra-pure inert atmosphere. The amorphous rods were prepared by overheating the melt at a controlled temperature substantially higher than the alloy liquidus temperature prior to quenching. Long-range residual stresses arising in as-quenched samples, that could substantially influence toughness, were eliminated during the extensive grinding of the rods in to rectangular shaped beams. The cracks were also generated near the centerline of the rods where residual stresses are essentially zero. Lastly, in order to eliminate the influence of any spatial or compositional variability that could be introduced by testing individually cast samples, several cast rods were produced and several specimens were extracted from each cast rod from various locations along the rod.

SAMPLE PREPARATION AND CONFIGURATIONAL STATE

CHARACTERIZATION

Three ingots of $Zr_{35}Ti_{30}Cu_{8.25}Be_{26.75}$ were prepared by weighing appropriate amounts of Zr (single crystal, 99.92% purity), Ti (single crystal, 99.99% purity), Cu (99.999% purity), and Be (99.9% purity). Each ingot was alloyed by arc melting in a Ti-gettered Argon atmosphere on a water-cooled copper hearth, and flipped at least four times to ensure chemical homogeneity. Three rods 8 mm in diameter with lengths varying

between 5 and 13 cm were produced by injection casting in a copper mold from the molten liquid state at 1100°C. Controlled melt heating was performed with RF induction power under argon atmosphere, and with the melt temperature being monitored by an infrared pyrometer. Four specimens extracted from a single rod were annealed and relaxed at different temperatures around the glass transition in order to investigate several relaxed states of the glass. Three specimens extracted from a single rod, and one more specimens extracted from another cast rod were investigated in their as-quenched state. The amorphous nature of all specimens was verified by X-ray diffraction with Cu K α radiation. The cylindrical rod segments were mechanically ground into ASTM E399 [14] single-edge-notch-bend rectangular bars that were 7 mm wide, 3.5 mm thick, and slightly longer than the testing span length of 28 mm. The specimen faces perpendicular to the crack were mirror polished with 0.02 μm colloidal silica. Notches having a length of 1 to 1.5 mm and a root radius of 125 μm were created on all samples using a wire saw with a 1 μm diamond slurry. Fatigue precracks were then created using a servo-hydraulic Materials Testing System MTS at a sinusoidal loading frequency of 10 Hz, R ratio of 0.1 and ΔK of $\sim 11 \text{ MPa}\cdot\text{m}^{1/2}$ while also never exceeding 60% of even the most brittle K_Q result. The combined length of the notch and fatigue precrack was ~ 3.5 mm on all samples, equal to the sample thickness in accordance with ASTM E399 [14]. Densities were measured using the Archimedes technique according to the ASTM standard C693 [15]. The room temperature shear and longitudinal wave speeds were measured using the pulse-echo overlap technique with 25 MHz ultrasound transducers. We note that the ultrasound measurements were taken right at the tip of the crack through the thickness of the sample in

order for the measurements to represent the average properties ahead of the crack tip plane. Using the data for the shear wave speed, longitudinal wave speed, and density ρ , the shear modulus G , bulk modulus B , and Poisson's ratio ν of the samples were calculated. Differential scanning calorimetry (DSC) using a Netzsch 404C calorimeter at a scan rate of $0.16 \text{ }^\circ\text{C}\cdot\text{s}^{-1}$ was performed using a small segment from each specimen to evaluate the glass transition temperature T_g and the associated recovered enthalpy ΔH at T_g .

The samples were relaxed by sealing them inside a quartz tube under an Argon atmosphere and annealing them for a sufficient amount of time for the glass to relax to a well-defined equilibrium liquid state. The four samples were annealed at the relaxation temperatures T_R of 280 °C, 300 °C, 320 °C, and 340 °C, which are just above and below the reported glass transition temperature T_g of 305 °C for $\text{Zr}_{35}\text{Ti}_{30}\text{Cu}_{8.25}\text{Be}_{26.7}$ [16]. The total annealing time for the 280 °C, 300 °C, 320 °C, and 340 °C samples at their respective temperatures is 520, 170, 41, and 15 minutes, respectively. The annealing of each sample was broken in to at least three annealing steps to ensure the samples do not crystallize and reach full equilibrium. The ρ , G , and B of each sample was measured after each annealing step, and equilibration was assessed by monitoring the relaxation of these variables [17]. X-ray diffraction was also performed after each annealing step to verify that the samples remain amorphous. The vibrational component (Debye-Grüneisen effect) of the moduli was not included in the reported moduli, as it is understood from prior work [12,17-19] that the configurational component of the moduli mostly controls the irreversible response of the liquid. However, we have included the calculation of the Debye-Grüneisen effect on the shear modulus and bulk modulus in appendix A, which contains the calculation of the

coefficient of thermal expansion and the measurement of the shear and longitudinal wave speeds at, and below, room temperature.

The measured ρ , G , B , and ν for the equilibrated and as-quenched states are listed in table 3.1. Across the relaxed states, G is shown to decrease very systematically with temperature, as expected by relaxing to increasingly higher and shallower potential energy wells in the glass landscape [12,17-19]. The decrease in G is by $\sim 4\%$, considerably outside the measurement error. On the other hand, B decreases by just $\sim 0.3\%$, well within the measurement error. Therefore, across the relaxed states where substantial configurational rearrangements take place, G more closely tracks these configurational rearrangements as compared to B . In this chapter, G will be regarded as the state variable quantifying the configurational state of the glass, as is widely understood to be directly proportional to the activation barrier to shear flow [12]. By plotting G vs. T_R in figure 3.1(a), a near linear relationship is observed, as expected from the work of Lind et al [17], we show the poor fitting of B vs. T_R in appendix B for contrast. The slope of the linear fit to the relaxed G vs. T_R is $-23.1 \text{ MPa}\cdot\text{C}^{-1}$. On the other hand, the data for the as-quenched specimens, which are superimposed in figure 3.1(a) as dashed lines extending across the entire temperature range, appear to be considerably less systematic and less consistent. Three of the samples display a G around 35 GPa with a rather small variance that is within the measurement error, suggesting a unique fictive temperature around 345 °C. The other sample displays a G that is appreciably higher than 35 GPa by a margin outside the measurement error, representing a higher fictive temperature, which is probably a consequence of spatially varying cooling conditions associated with the copper mold casting process.

The recovered enthalpy ΔH , which is understood to be directly related to the configurational energy of the metallic glass [18] will be used here as an independent variable quantifying the configurational state of the glass. The recovered enthalpies were calculated in reference to the as-quenched sample that displayed the lowest value of ΔH . The DSC scans performed at $0.16 \text{ }^\circ\text{C}\cdot\text{s}^{-1}$ that were used in determining the relative values of ΔH are shown in appendix C. The ΔH data are listed in table 3.1 and plotted vs. T_R in figure 3.1(b). Like with G , the ΔH values for the relaxed states decrease very systematically and consistently with T_R over a rather broad range. A linear fit to the data reveals a slope of $-6.6 \text{ J}/(\text{mol}\cdot^\circ\text{C})$. On the other hand, the ΔH data for the as-quenched states closely resemble the behavior displayed by the G data, with three of the data suggesting a rather unique fictive temperature along with an outlying data point. By plotting G vs. ΔH in figure 3.1(c), a good correlation between G and ΔH is found, which even extends through the anomalous as-quenched data point. The near linear relationship reflects the one-to-one correspondence between G and ΔH independent of the fictive temperature. The linear fit to all samples reveals a slope of $dG/d\Delta H = 3.07 \times 10^{-7} \text{ m}^3/\text{mol}$. The tight G vs. ΔH correlation confirms that the average measured shear modulus accurately reflects the configurational enthalpy of the associated glass state, a concept that forms the basis for the cooperative shear model describing shear flow activation in metallic glass [12].

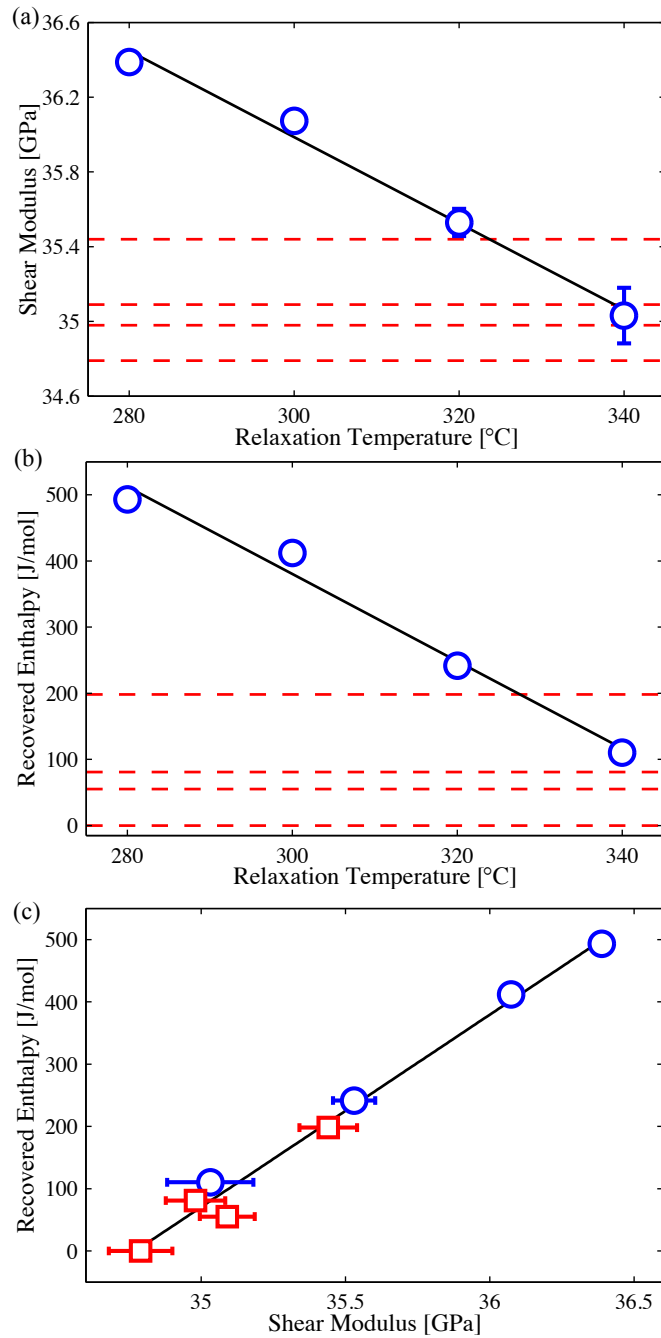


Figure 3.1 (a) Shear modulus G (with associated measurement error) vs. relaxation temperature T_R and (b) recovered enthalpy ΔH vs. relaxation temperature T_R for equilibrated $Zr_{35}Ti_{30}Cu_{8.25}Be_{26.75}$ samples (blue circles). The lines are linear fits through the data, and the extended dashed lines correspond to the values for the three as-quenched

$Zr_{35}Ti_{30}Cu_{8.25}Be_{26.75}$ samples. (c) Shear modulus G (with associated measurement error) vs. recovered enthalpy ΔH for both equilibrated (blue circles) and as-quenched (red squares) $Zr_{35}Ti_{30}Cu_{8.25}Be_{26.75}$ samples.

FRACTURE TOUGHNESS TESTING

Square beams with a side length of ~ 3.5 mm and an aspect ratio of ~ 2 were sectioned from the fracture toughness specimens post fracture within millimeters of the notch and were polished plane parallel for compression testing. The stress vs. strain response was measured at a strain rate of 10^{-3} s^{-1} in an Instron load frame, and the yield strength σ_y was assessed. The measured σ_y values, shown in table 1, show practically no variation. While this is not particularly useful in terms of revealing a correlating tendency, we can use the average σ_y to calculate the limiting value that can be considered as valid plane strain fracture toughness, K_{IC} , according to ASTM E399 [14]. Plane strain and small-scale yielding conditions are ensured when certain sample dimensions (total crack length, uncracked ligament length, and the out-of-crack-plane thickness) are greater than or equal to $5K_Q^2/2\sigma_y^2$. We estimate that for the present samples, any fracture toughness less than or equal to $64 \text{ MPa}\cdot\text{m}^{1/2}$ can be considered a valid K_{IC} measurement.

The fracture toughness tests were carried out in three-point bending mode on a MTS load frame at a constant displacement rate of 0.3 mm/min. The critical stress intensity K_Q was calculated from the critical load according to ASTM E399 [14], and is listed in table 1 for each sample. Three of the eight K_Q values slightly exceeded the K_{IC}

valid cutoff of $64 \text{ MPa}\cdot\text{m}^{1/2}$. The fracture toughness values in the relaxed states are found to vary broadly from 26 to $74 \text{ MPa}\cdot\text{m}^{1/2}$ over the T_R range considered. More interestingly, the fracture toughness in the as-quenched states are found to vary even more broadly, ranging from 31 to $110 \text{ MPa}\cdot\text{m}^{1/2}$ between the five tests, with an average of $75 \text{ MPa}\cdot\text{m}^{1/2}$ and a standard deviation of $35 \text{ MPa}\cdot\text{m}^{1/2}$. Images of the fracture surfaces were taken with a LEO 1550VP field emission scanning electron microscope SEM. The relaxed states fracture surfaces are shown in figure 3.2 and the as-quenched fracture surfaces are shown in figure 3.3. The LEO SEM was also used to investigate compositional contrast in the samples with backscattered electron images and energy dispersive X-ray spectroscopy EDS. No evidence of contrast was found with either technique. This, together with the absence of any cleavage fracture region in the vicinity of the pre-crack, suggest that fracture was likely not triggered by entrained oxide inclusions in any of the samples tested here [8]. Therefore it appears that fracture has been accommodated entirely by a shear process, even in the most brittle cases. During fracture, the shear banding process produces a jagged and rough fracture surface zone ahead of the crack tip, whose degree and extent is expected to correlate with the associated plastic zone radius determined by $K_Q^2/\pi\sigma_y^2$ [9]. The sample fracture toughness and surface roughness in both figure 3.2 and figure 3.3 increases as the images go from top to bottom.

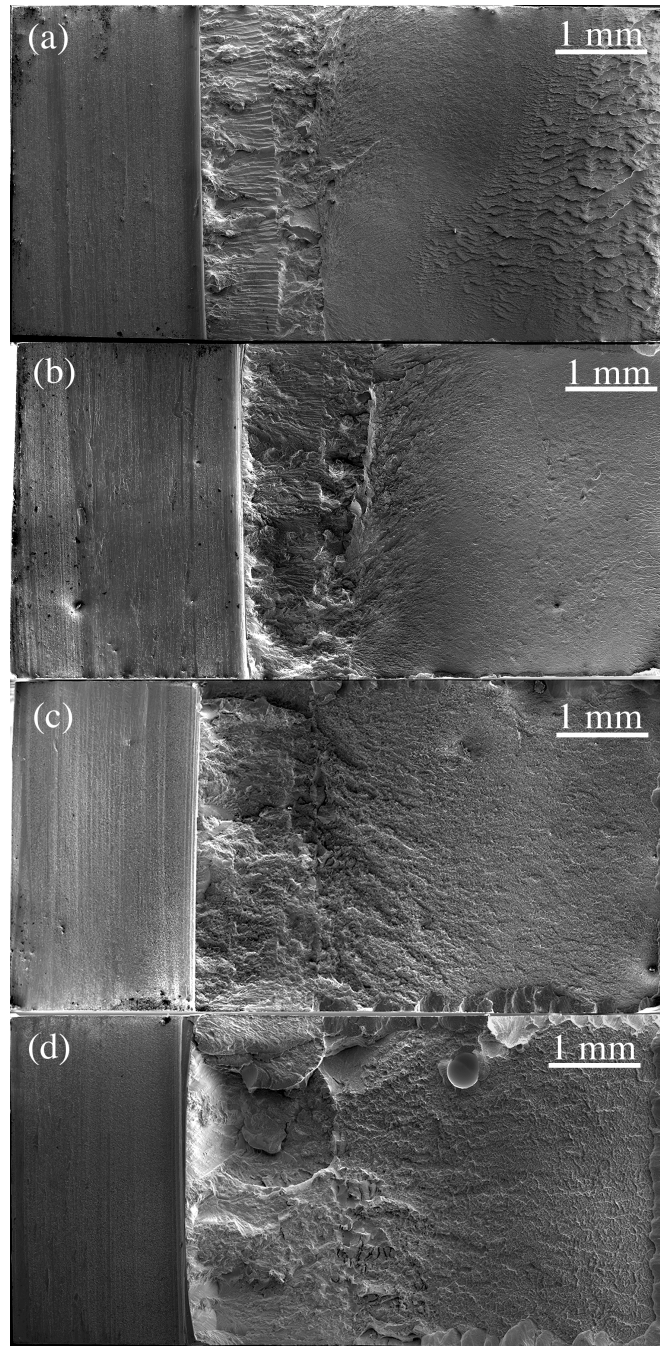


Figure 3.2 Scanning electron micrographs of the fracture surfaces from $\text{Zr}_{35}\text{Ti}_{30}\text{Cu}_{8.25}\text{Be}_{26.75}$ fracture toughness samples relaxed, prior to fracture, at (a) $280\text{ }^{\circ}\text{C}$ $K_Q = 26\text{ MPa}\cdot\text{m}^{1/2}$, (b) $300\text{ }^{\circ}\text{C}$ $K_Q = 36\text{ MPa}\cdot\text{m}^{1/2}$, (c) $320\text{ }^{\circ}\text{C}$ $K_Q = 61\text{ MPa}\cdot\text{m}^{1/2}$, and (d) $340\text{ }^{\circ}\text{C}$ $K_Q = 74\text{ MPa}\cdot\text{m}^{1/2}$.

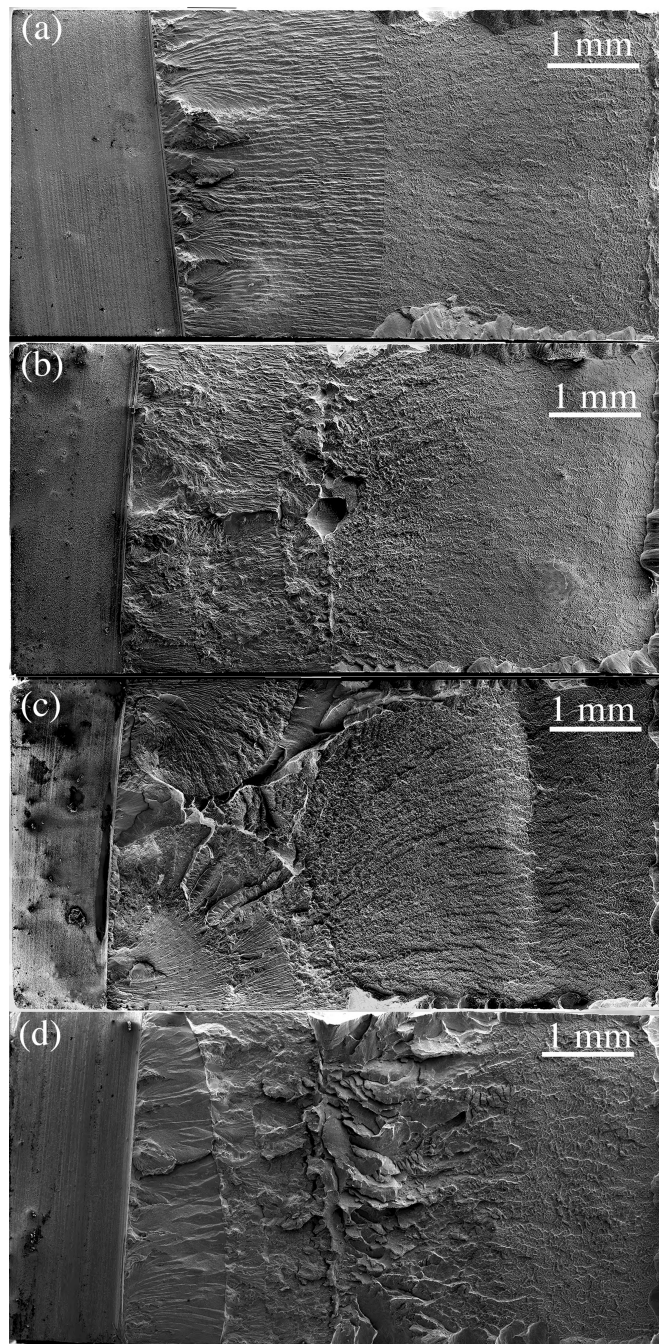


Figure 3.3 Scanning electron micrographs of the fracture surfaces from $\text{Zr}_{35}\text{Ti}_{30}\text{Cu}_{8.25}\text{Be}_{26.75}$ fracture toughness samples tested in their as-quenched state: (a) $K_Q = 62 \text{ MPa}\cdot\text{m}^{1/2}$, (b) $K_Q = 96 \text{ MPa}\cdot\text{m}^{1/2}$, (c) $K_Q = 31 \text{ MPa}\cdot\text{m}^{1/2}$, and (d) $K_Q = 110 \text{ MPa}\cdot\text{m}^{1/2}$.

Table 3.1 Data for the density ρ , shear modulus G , bulk modulus B , Poisson's ratio ν , recovered enthalpy ΔH , yield strength σ_y , glass-transition temperature T_g , and fracture toughness K_Q for the $Zr_{35}Ti_{30}Cu_{8.25}Be_{26.75}$ samples in various relaxed states at temperatures T_R as well as in their as-quenched state.

Sample State	ρ [g/cm ³]	G [GPa]	B [GPa]	ν [—]	ΔH [J/mol]	σ_y [MPa]	T_g [°C]	K_Q [MPa·m ^{1/2}]
280°C Relaxed	5.378	36.39	105.8	0.3457	493	1700	303	26
300°C Relaxed	5.376	36.07	105.8	0.3469	412	1680	300	36
320°C Relaxed	5.373	35.53	105.6	0.3488	242	1710	298	61
340°C Relaxed	5.367	35.03	105.4	0.3505	110	1700	298	74
As-quenched	5.366	35.44	104.9	0.3482	198	1690	301	62
As-quenched	5.368	34.98	104.6	0.3495	81	1630	304	96
As-quenched	5.379	35.09	106.0	0.3509	55	1680	304	31
As-quenched	5.396	34.79	104.9	0.3507	0	1700	309	110

In figure 3.4(a) and 3.4(b) we plot K_Q vs. G and ΔH respectively. The fracture toughness of the relaxed samples varies very systematically with both G and ΔH , displaying a near linear relationship. A linear fit to the K_Q vs. G data reveals a slope of $-37.1 \text{ MPa}\cdot\text{m}^{1/2}/\text{GPa}$, suggesting that for each gigapascal the shear modulus is lowered, the fracture toughness is increased by $\sim 37 \text{ MPa}\cdot\text{m}^{1/2}$. A linear fit to the K_Q vs. ΔH data reveals a slope of $-0.13 \text{ MPa}\cdot\text{m}^{1/2}\cdot\text{mol}/\text{J}$ and implies that for each 100 J/mol the configurational enthalpy is increased, the fracture toughness is increased by $\sim 13 \text{ MPa}\cdot\text{m}^{1/2}$. On the other hand, the fracture toughness values corresponding to the as-quenched samples display no correlating tendency with either G or ΔH . In fact, none of the measured properties listed in table 3.1 had any correlating tendency with the fracture toughness of the as-quenched glass. We plot K_Q vs. bulk modulus B and Poisson ratio ν in appendix B to

show that there is indeed no correlating tendency for even the often used Poisson ratio [20] for the as-quenched samples.

To exemplify the effect of disorder on toughness, we focus on the relaxed sample displaying a shear modulus of ~ 35 GPa and recovered enthalpy of ~ 110 J/mol, as these values roughly compare to the G and ΔH values of the as-quenched samples (excluding the outlying as-quenched data). The near equivalent shear modulus of ~ 35 GPa and recovered enthalpy of ~ 110 J/mol between the relaxed and as-quenched samples implies a near equivalent fictive temperature for all samples, which appears to be ~ 345 °C from figures 3.1(a) and 3.1(b). One would reasonably expect that since all samples, as-quenched or relaxed, have about the same glass configurational state, as evidenced by the near equivalent average configurational properties, they should exhibit about the same fracture toughness. However, fracture toughness varies enormously between these samples. The as-quenched samples demonstrate a fracture toughness ranging between 31 and $110 \text{ MPa}\cdot\text{m}^{1/2}$, with an average of $75 \text{ MPa}\cdot\text{m}^{1/2}$ and variance of $35 \text{ MPa}\cdot\text{m}^{1/2}$. The relaxed sample demonstrates a fracture toughness of $74 \text{ MPa}\cdot\text{m}^{1/2}$, which is very close to the average value of the as-quenched specimens. The very large variance in the toughness between samples cannot be explained by the presence of oxygen, impurities, or inclusions in some of the samples and absence in others, or by compositional variance or any kind of gradients along the centerline of the cast rods. The as-quenched samples with K_Q of 31, 62 and $96 \text{ MPa}\cdot\text{m}^{1/2}$ were extracted from the same cast rod (top, bottom and middle segments of the rod respectively), while the as-quenched sample with K_Q of $110 \text{ MPa}\cdot\text{m}^{1/2}$ and the relaxed sample with K_Q of $74 \text{ MPa}\cdot\text{m}^{1/2}$ were each extracted from a different rod (bottom

and top segments of the rods respectively). Moreover, the EDS analysis verifies a chemical homogeneity across samples, while the absence of any visible cleavage fracture region in the fractography of the samples (particularly the brittle ones) precludes any significant influence by inclusions.

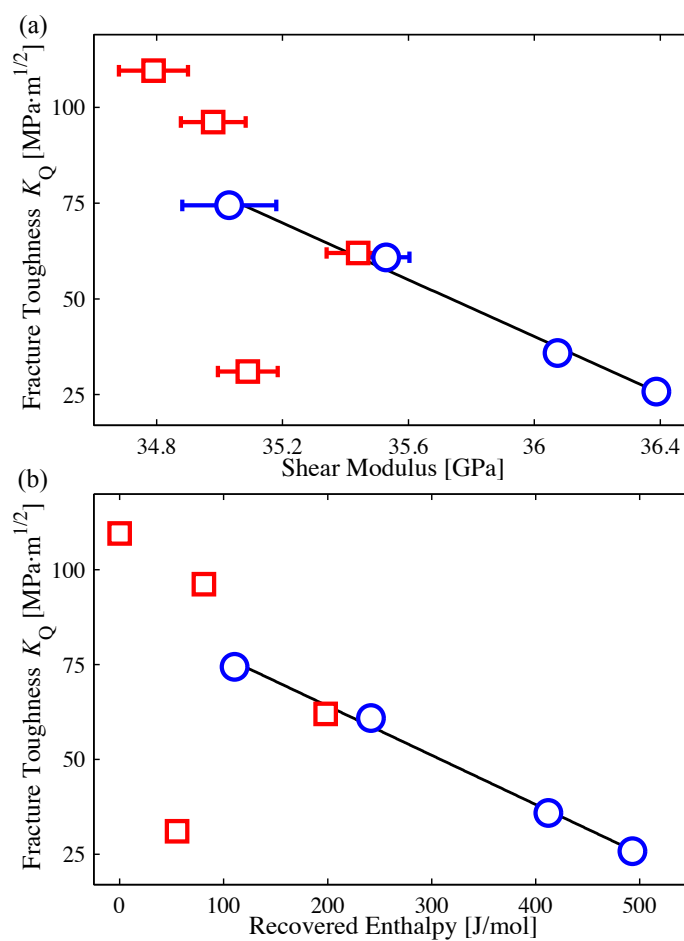


Figure 3.4 (a) Fracture toughness K_Q vs. shear modulus G (with associated measurement error) and (b) fracture toughness K_Q vs. recovered enthalpy ΔH for equilibrated (blue circles) and as-quenched (red circles) $Zr_{35}Ti_{30}Cu_{8.25}Be_{26.75}$ samples. The lines are linear fits through the data for the equilibrated samples.

The broad toughness variance in that as-quenched state and the lack of any correlating tendency between K_Q and G or ΔH lends support to the concept that a large configurational disorder dominates the fracture process in the as-quenched state. Fracture is not a global process but a local one, and can be sensitive to length scales that could be as small as the glass short-range order. Specifically, the rate of extension of a pre-existing crack, whose tip is essentially atomically sharp, could be heavily influenced by the compliance of the local shear transformation zones (STZs) in the immediate vicinity of the crack tip. As recently revealed by means of acoustic force atomic microscopy, the variance in the STZ moduli in the as-quenched state is expected to be rather large [21]. A large configurational disorder increases the probability that the majority of configurational fluctuations in the immediate vicinity of an existing precrack could either be highly susceptible to shear transformation, or highly resistant to it, giving rise to a non-unique fracture resistance associated with a given average glass configuration. This is because the crack tip is essentially a one dimensional line traversing the sample across its width, and the distribution of the STZ environment ahead of the crack tip would not necessarily be representative of the bulk sample. If the distribution in the bulk sample is rather broad, the local distribution in the crack tip environment can be skewed either towards softer or harder STZs. Soft and highly compliant STZs would encourage plastic rearrangement ahead of the crack tip, suppressing fracture instability and promoting stable crack growth. Hard and stiff STZs would give rise to large and highly localized stresses ahead of the crack tip, promoting fracture instability and leading to unstable crack growth. Therefore, the large variance in STZ modulus in the as-quenched state could produce a fracture toughness that

may be considerably higher or considerably lower than the mean. By equilibrating the glass to a well-defined configurational state, the frozen-in STZ configurations that are largely responsible for the large configurational disorder are allowed to relax, thereby narrowing the modulus variance. The resistance to crack propagation is then influenced by a local STZ environment that is likely representative of the bulk material, and as such, the fracture toughness is determined by the mean configurational properties rather than dominated by their variance. Accordingly, the toughness of a relaxed glass correlates strongly with the average configurational state variables (i.e., G and ΔH), and the fracture process becomes more deterministic and more predictable.

In addition, it would be instructive to focus on the origin of the large configurational disorder in an as-quenched glass as compared to a glass relaxed at an equivalent fictive temperature. From an equilibrium thermodynamics consideration, two glasses that fall out of equilibrium at the same temperature and pressure should exhibit essentially identical configurational properties distributed over approximately the same mean and variance. However, by considering kinetics, which are dominant during dynamic vitrification of a glass, and recognizing that the glass vitrification process evolves over a spectrum of fluctuations rather than by a single fluctuational event, one can reasonably expect a rather large degree of disorder in an as-quenched glass. A relaxation map of a typical metallic glass is shown in figure 3.5 [22,23]. A schematic exemplifying the spectrum of relaxations over a range of frequencies at constant temperature is presented in figure 3.5(a), and one showing the spectrum of relaxations over a range of temperatures at constant frequency is presented in figure 3.5(b). The quenching of a high temperature melt

is a highly dynamic process occurring over a range of temperatures and frequencies, instead of a unique temperature and frequency. Hence, it is conceivable that a spectrum of

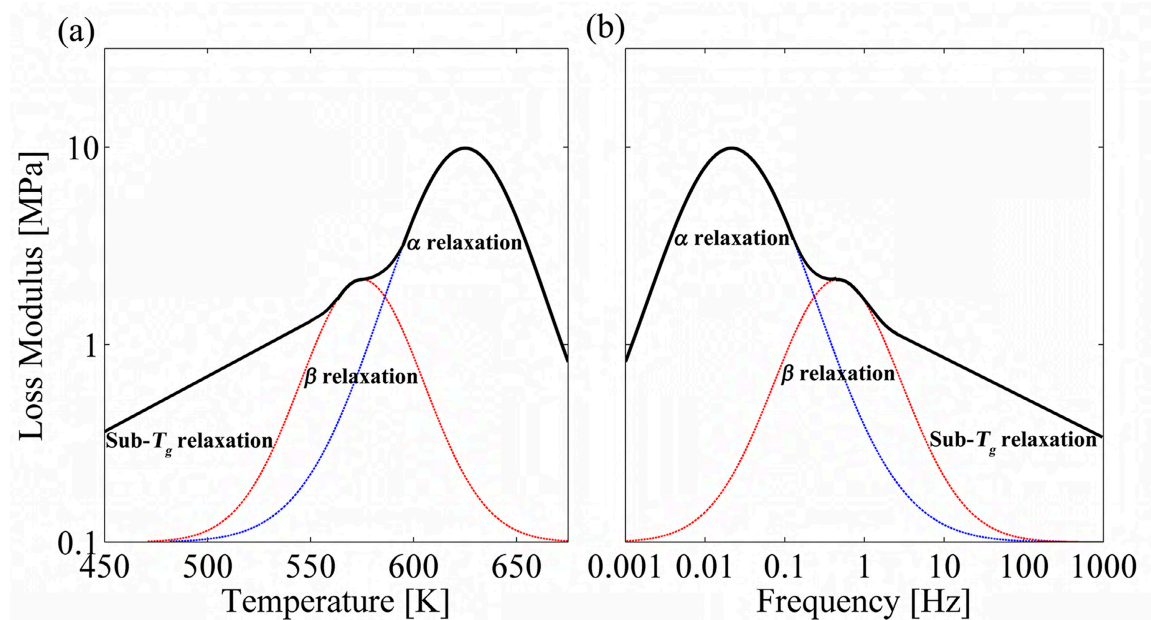


Figure 3.5 Relaxation map of a typical metallic glass [22,23]. (a) Loss modulus vs. frequency at constant temperature; (b) Loss modulus vs. temperature at constant frequency. Approximate distributions for the slow α modes, fast β modes, and ultra-fast sub- T_g modes are designated.

unrelaxed modes would be captured during such a dynamic process, including fast modes (some of which may be β modes) captured at lower temperatures and higher frequencies, and slow modes captured at higher temperatures and lower frequencies. Ahead of a stressed crack tip, those fast modes would act as the more compliant modes that encourage plastic rearrangement and stable crack growth, while the slow modes would act as the stiffer modes that promote fracture instability and unstable crack growth. In contrast, when

relaxing an as-quenched glass to an equilibrium state of equivalent potential energy, the relaxation process occurs at a well-defined temperature and essentially zero frequency. As such, the slower modes captured at higher temperatures and the faster modes captured at higher frequencies would relax, leading to a significantly narrower equilibrium distribution of unrelaxed modes captured in the relaxed glass. Consequently, a relaxed glass would be spatially more homogeneous at the length scale of its short-range order, such that it would exhibit a more deterministic and more predictable fracture resistance.

Aside from demonstrating that relaxation of the metallic glass to a well-defined configurational state leads to a predictable and reliable toughness, the present results further elucidate the underlying thermodynamics controlling toughness and point to interesting technological implications. As we noted earlier, figure 3.4(b) reveals that increasing the configurational enthalpy of a relaxed sample linearly increases toughness at a ratio of $13 \text{ MPa}\cdot\text{m}^{1/2}$ per 100 J/mol . Although it is not evident from figure 3.4(b) that the increase in toughness with configurational enthalpy will remain linear at very high ΔH values rather than saturating at some limiting value, one can envision increasing the configurational enthalpy of a metallic glass by many kJ/mol and gaining substantial toughness on the order of hundreds of $\text{MPa}\cdot\text{m}^{1/2}$. Conventional thermal annealing treatments are limited by an inability to freeze in the high temperature configurational state because of either intervening crystallization or the relaxation rate becoming higher than the quench rate. However, if large increases in the configurational enthalpy of a relaxed sample can be translated into large gains in toughness, as figure 3.4(b) suggests, the technological implications could be of great engineering interest. In figure 3.6 we present a performance

map of toughness vs. strength (Ashby map) showing the strength and toughness relationship of metallic glasses alongside conventional engineering metals. The toughness and strength data obtained for the four relaxed states in this work are superimposed on the plot (the arrow points in the direction of increasing configurational enthalpy). As seen in the plot, a potential for very high toughness exists for metallic glasses that could attain very high configurational enthalpies, perhaps far surpassing the benchmark toughness values achieved by the toughest engineering metals known.

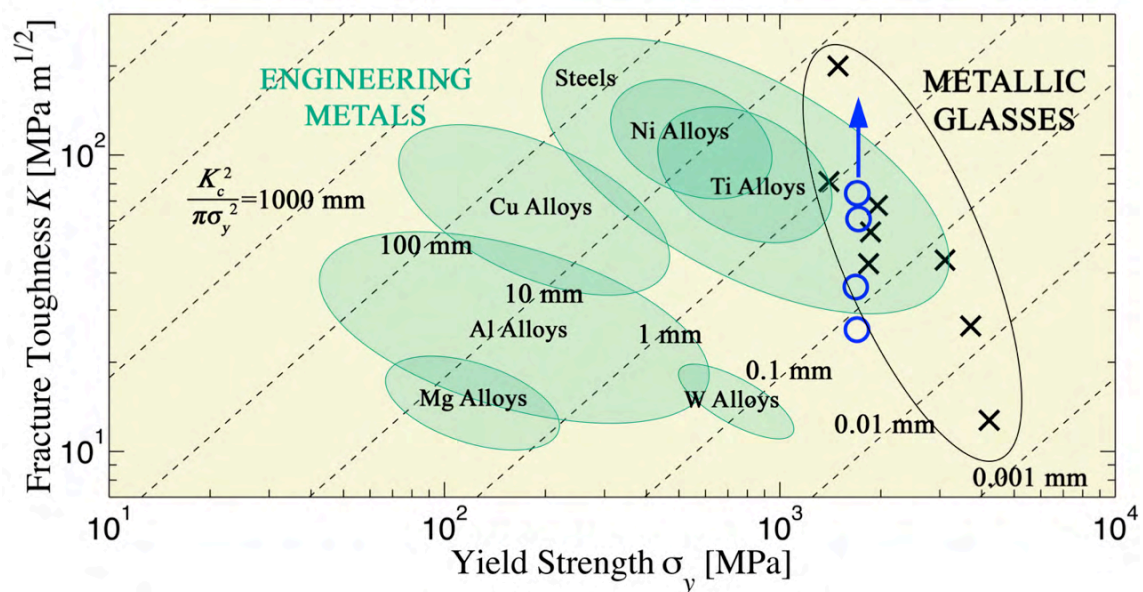


Figure 3.6 Ashby map of fracture toughness K_Q vs. yield strength σ_y in the damage tolerance range of engineering alloys. The green shaded ovals represent common crystalline engineering metals [24] and the black oval represents metallic glasses. The black crosses are metallic glasses taken from Demetriou et al. [1]. The blue circles are the annealed $Zr_{35}Ti_{30}Cu_{8.25}Be_{26.75}$ samples from this letter. The blue arrow indicates the increase in damage tolerance made possible by further increasing the configurational enthalpy of the metallic glass.

BIBLIOGRAPHY

- [1] M. D. Demetriou, M. E. Launey, G. Garrett, J. P. Schramm, D. C. Hofmann, W. L. Johnson, and R. O. Ritchie, *Nat Mater* **10**, 123 (2011).
- [2] R. O. Ritchie, *Nat Mater* **10**, 817 (2011).
- [3] X. J. Gu, S. J. Poon, G. J. Shiflet, and J. J. Lewandowski, *Acta Mater* **58**, 1708 (2010).
- [4] P. A. Hess, S. J. Poon, G. J. Shiflet, and R. H. Dauskardt, *Journal of Materials Research* **20**, 783 (2005).
- [5] A. Kawashima, H. Kurishita, H. Kimura, and T. Zhang, *Materials Transactions* **46**, 1725 (2005).
- [6] J. H. Schneibel, J. A. Horton, and P. R. Munroe, *Metall and Mat Trans A* **32**, 2819 (2001).
- [7] A. Shamimi Nouri, X. J. Gu, S. J. Poon, G. J. Shiflet, and J. J. Lewandowski, *Philosophical Magazine Letters* **88**, 853 (2008).
- [8] S. V. Madge, D. V. Louzguine-Luzgin, J. J. Lewandowski, and A. L. Greer, *Acta Mater* **60**, 4800 (2012).
- [9] J.-Y. Suh, R. D. Conner, C. P. Kim, M. D. Demetriou, and W. L. Johnson, *Journal of Materials Research* **25**, 982 (2010).
- [10] H. Kimura and T. Masumoto, *Acta Metallurgica* **28**, 1677 (1980).
- [11] J. J. Lewandowski, *Materials Transactions* **42**, 633 (2001).
- [12] M. D. Demetriou, J. S. Harmon, M. Tao, G. Duan, K. Samwer, and W. L. Johnson, *Phys Rev Lett* **97**, (2006).
- [13] C. Rycroft and E. Bouchbinder, *Phys Rev Lett* **109**, 194301 (2012).
- [14] *ASTM Standard E399* (ASTM International, West Conshohocken, PA, 2012).
- [15] *ASTM Standard C693*, 2008 ed. (ASTM International, West Conshohocken, PA, 2008).
- [16] G. Duan, A. Wiest, M. L. Lind, J. Li, W.-K. Rhim, and W. L. Johnson, *Adv Mater* **19**, 4272 (2007).

- [17] M. L. Lind, G. Duan, and W. L. Johnson, *Phys Rev Lett* **97**, 015501 (2006).
- [18] W. L. Johnson, M. D. Demetriou, J. S. Harmon, M. L. Lind, and K. Samwer, *Mrs Bull* **32**, 644 (2007).
- [19] J. S. Harmon, M. D. Demetriou, W. L. Johnson, and K. Samwer, *Phys Rev Lett* **99**, (2007).
- [20] J. J. Lewandowski, W. H. Wang, and A. L. Greer, *Philosophical Magazine Letters* **85**, 77 (2005).
- [21] H. Wagner, D. Bedorf, S. Kuechemann, M. Schwabe, B. Zhang, W. Arnold, and K. Samwer, *Nat Mater* **10**, 439 (2011).
- [22] K. L. Ngai, *Relaxation and Diffusion in Complex Systems* (Springer New York, New York, NY, 2011).
- [23] H. B. Yu, K. Samwer, Y. Wu, and W. H. Wang, *Phys Rev Lett* **109**, 095508 (2012).
- [24] M. F. Ashby, *Materials Selection in Mechanical Design* (Pergamon Press, Oxford; New York, 1992).